



Magnetoresistance and spin electronics

A. Barthélémy^{a,*}, A. Fert^a, J-P. Contour^a, M. Bowen, V. Cros^a, J.M. De Teresa^a,
A. Hamzic^a, J.C. Faini^b, J.M. George^a, J. Grollier^a, F. Montaigne^a, F. Pailloux^a,
F. Petroff^a, C. Vouille^a

^a *Unité Mixte de Physique CNRS-Thales, Domaine de Corbeville, 91404 Orsay, France*

^b *L2M-CNRS, 92250 Bagneux, France*

Abstract

We review several topics in the field of spin electronics: (i) giant magnetoresistance observed in magnetic multilayers; (ii) magnetization reversal by spin injection and (iii) spin-polarized tunneling in magnetic tunnel junctions combining electrodes of ferromagnetic transition metal and half-metallic oxide. © 2002 Elsevier Science B.V. All rights reserved.

Keywords: Giant magnetoresistance; Spin injection; Tunnel junctions

1. Introduction

Spin electronics or spintronics is a new field of electronics which is not based on the conduction by electrons or holes as in semiconductor devices but relies on the different transport properties of the majority spin and minority spin electrons. In fact, spintronics results from the spin dependence of the conduction in ferromagnetic metals which can be exploited in magnetic nanostructures such as multilayers or magnetic tunnel junctions to obtain properties depending on the applied magnetic field such as giant magnetoresistance (GMR) or tunnel magnetoresistance (TMR).

These spin electronic phenomena have been applied rapidly since the first observation of GMR had been reported in 1988 and magnetic sensors and read heads based on this effect are available since 1994 and 1997, respectively.

We will describe some of the effects of spin electronics taking example from the work we have performed in Albert Fert's group in Orsay.

2. Giant magnetoresistance

GMR was discovered in 1988 on Fe/Cr magnetic multilayers [1], that is a stack of Fe and Cr layers with individual thicknesses of the order of 1 nm. In these multilayers, for certain thicknesses of the Cr interlayer, the magnetizations of adjacent Fe layers are antiparallelly oriented by an antiferromagnetic interlayer exchange coupling [2]. By application of a magnetic field, the resistance of the multilayer decreases drastically, as shown in Fig. 1, when the magnetizations of the two layers progressively align in the direction of the field. The GMR ratio, defined as $GMR = (R^{AP} - R^P)/R^P$, where $R^{P(AP)}$ is the resistance in the parallel (antiparallel) state, is 80% at helium temperature and 20% at room temperature when the thickness of Cr is 9 Å. A record GMR effect of 220% has been reported by Shad et al. [3]. GMR effects have been reported in a large number of systems combining ferromagnetic transition metal or alloys with nonmagnetic metals (for a review, see Ref. [4]). The variation of the GMR with the thickness of the nonmagnetic layer is oscillatory [5], which reflects the thickness dependence of the magnetic coupling. The antiparallel (AP) configuration can also be obtained in multilayers in which consecutive magnetic layers have different coercivities [6], or by combining hard and soft magnetic layers. The best-known structure to obtain an AP arrangement is the

*Corresponding author. Tel.: +33-1693-39381; fax: +33-1693-30740.

E-mail address: agnes.barthelemy@thalesgroup.com (A. Barthélémy).

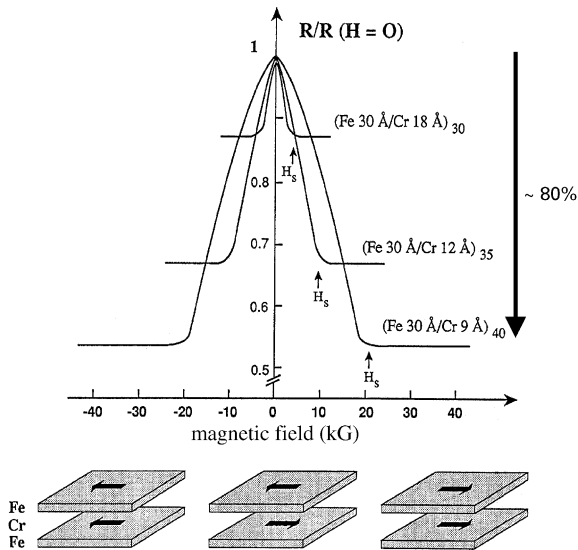


Fig. 1. Magnetoresistance curves at 4.2 K of (Fe/Cr) multilayers [1].

spin valve structure [7]. In this case, the multilayer is composed of a soft magnetic layer separated by a non magnetic layer from a hard magnetic layer obtained by pinning by an exchange bias interaction with an antiferromagnetic or ferrimagnetic layer such as FeMn. When the magnetic field is increased from negative to positive values, the magnetization of the free layer reverses in a very small field (a few oersteds), while the magnetization of the pinned layer remains fixed. The consecutive steep increase of the resistance in small field obtained in this way is now used for many low-field applications such as magnetic sensors, read heads or Magnetic Random Access Memories.

GMR effects have been obtained in two geometries. In the first one the current is applied in the plane of the layer (hereafter denoted CIP), as in the experiments described above, while in the second one the current flows perpendicular to the plane of the layers (hereafter denoted CPP). The first measurements, in this last configuration, have been obtained by sandwiching the multilayer between two superconducting Nb layers [8]. CPP-GMR configuration has also been obtained in nanowires, that is multilayers electrodeposited in the pores of a nuclear track-etched polycarbonate membranes [10], or by oblique deposition on a prestructured substrate [11]. As in the CIP geometry, the dependence of the GMR ratio on the nonmagnetic thickness exhibits an oscillatory behavior as shown in Fig. 2. From this figure, it turns out that the CPP-GMR is definitely larger than the CIP-GMR and exists at much larger thicknesses. These differences are due to the two different scaling lengths of the problem. Whereas the scaling

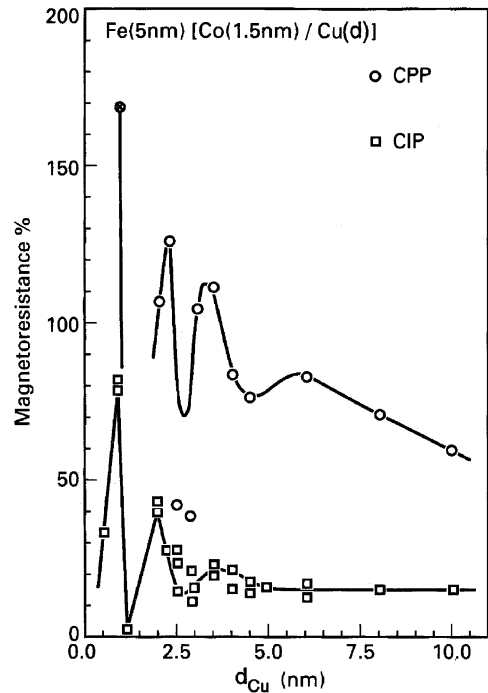


Fig. 2. Variation of the CPP and CIP GMR as a function of the nonmagnetic Cu thickness [9].

length of the CIP geometry is the mean free path λ , due to spin accumulation effects, the scaling length of the CPP geometry is the spin diffusion length, l_{sf} , which is ten times larger than the mean free path.

The GMR is related to the spin dependence of the conduction in ferromagnetic metals and alloys. This spin dependence arises from the unbalance of the spin populations at the Fermi level (due to the splitting of the d bands) which induces different probabilities of the $s \rightarrow d$ transition for majority spin (spin parallel to the magnetization or spin \uparrow) and minority spins (spin antiparallel to the magnetization or spin \downarrow), and consequently different resistivities for spin \uparrow and spin \downarrow electrons. At low temperature, in ferromagnetic metals, the current is carried by two independent channels of carriers, one for spin \uparrow electrons with a resistivity ρ_{\uparrow} , and the other made of spin \downarrow electrons with a resistivity ρ_{\downarrow} . The spin asymmetry of the resistivities of the two channels is characterized by the coefficient $\alpha = \rho_{\downarrow}/\rho_{\uparrow}$ or $\beta = (\rho_{\uparrow} - \rho_{\downarrow})/(\rho_{\uparrow} + \rho_{\downarrow})$.

The mechanism of the GMR is illustrated in Fig. 3 in the case where $\alpha > 1$, that is the resistivity smaller for the majority spins. In the parallel (P) configuration, the spin $+$ electrons are always the majority spin electrons and then always weakly scattered in all the layers resulting in a resistance r smaller for this channel than the resistance R of the spin $-$ channel. The shorting of

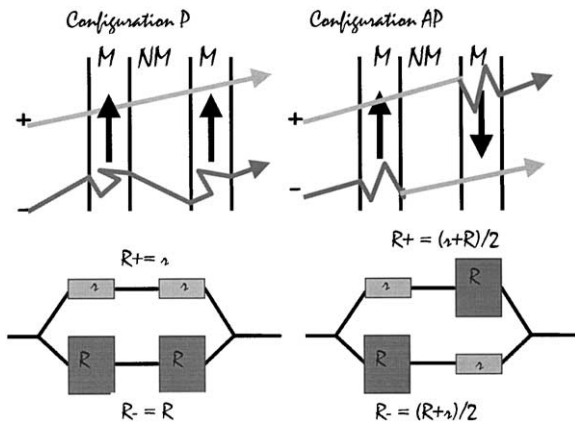


Fig. 3. Schematic picture of the GMR mechanism. The electron trajectory between two scatterings are represented by straight lines and the scattering by abrupt change in the direction. The signs + and - are for spins $S_z = \frac{1}{2}$ and $-\frac{1}{2}$, respectively. The arrows represent the majority spin direction in the magnetic layers.

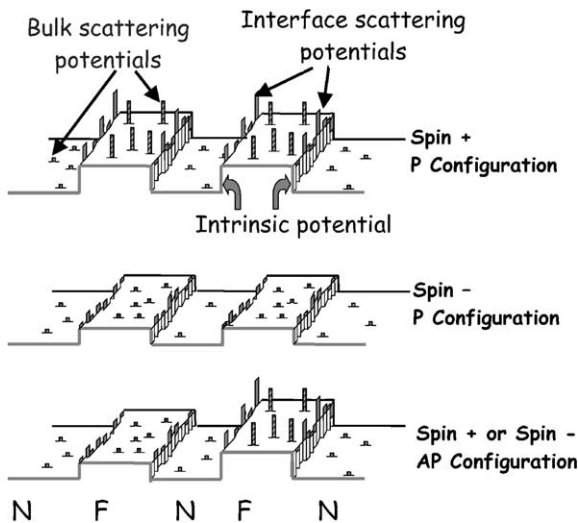


Fig. 4. Potential landscape seen by spin+ and spin- conduction electrons in the P and AP configurations. The intrinsic potential is represented by a periodic array of steps. The bulk and interface scattering potentials are represented by spikes.

the current by this fast electron channel makes the resistivity low in the P state ($R_P = r$). In the AP configuration, each of the spin directions is alternately the majority and the minority one. The resistance is averaged in each channel and the whole resistance $R_{AP} = (r + R)/4$ is larger than in the P state. The GMR ratio is defined as $GMR = (R_{AP} - R_P)/R_P = (r - R)^2/4rR$. This picture holds in the CIP and CPP geometries when the thicknesses are smaller than the scaling length, that is the mean free path in CIP

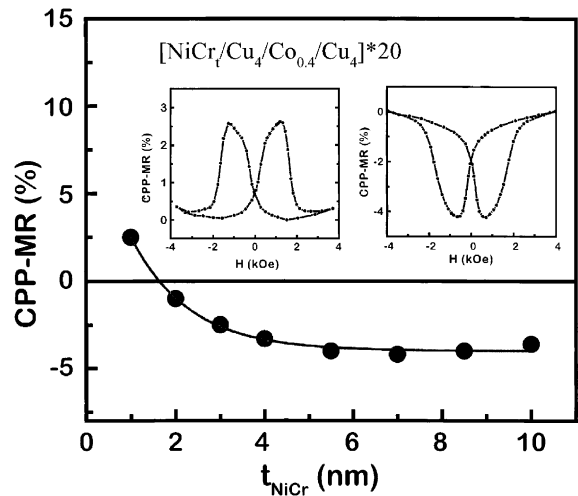


Fig. 5. Variation of the CPP-GMR as a function of the thickness of the $Ni_{0.95}Cr_{0.05}$ layers in NiCr/Cu/Co multilayers. The competition between the bulk scattering (characterized by $\beta_{NiCr} < 0$) and the interface scattering (with $\gamma_{NiCr/Cu} > 0$) gives rise to a compensation thickness at which they cancel each other. Below this compensation thickness, the interface scattering is preponderant and the global spin asymmetry of the NiCr/Cu layer is positive as that of the Co/Cu layer, the resulting effects are then normal (see (a)). Above the critical thickness, the bulk scattering becomes predominant so that the global asymmetry is negative and opposite to that of the Co/Cu layer. The resulting effect is then inverse (b) [12].

and the spin diffusion length in CPP. The microscopic origin of the GMR is well represented by the potential landscape seen by the conduction electrons represented in Fig. 4. In this potential, two contributions can be distinguished. The first one is the intrinsic potential which is the potential of the perfect multilayer which reflect the band mismatch between the magnetic and nonmagnetic layers. It is periodic for a periodic multilayer. The exchange splitting of the d_{\uparrow} and d_{\downarrow} bands in the ferromagnetic layers results in different heights of the steps seen by spin \uparrow and spin \downarrow conduction electrons. In the P configuration, the height of the steps is the same in all the layers but different for majority and minority spins. In the AP state, small and large steps alternate for each spin direction. The second contribution arises from the extrinsic potential associated to the presence of impurities in the layers or to the roughness at the interfaces. They are represented by spikes in the figure. Since in ferromagnetic metals, the scattering is spin dependent, we have different scattering potentials for the majority and minority spin electrons. Both extrinsic and intrinsic potential generate GMR in CIP and CPP geometries and it is difficult to separate them. The most spectacular example of impurity effect (extrinsic potential) on GMR has been obtained in $(F/Cu/Co/Cu)_N$

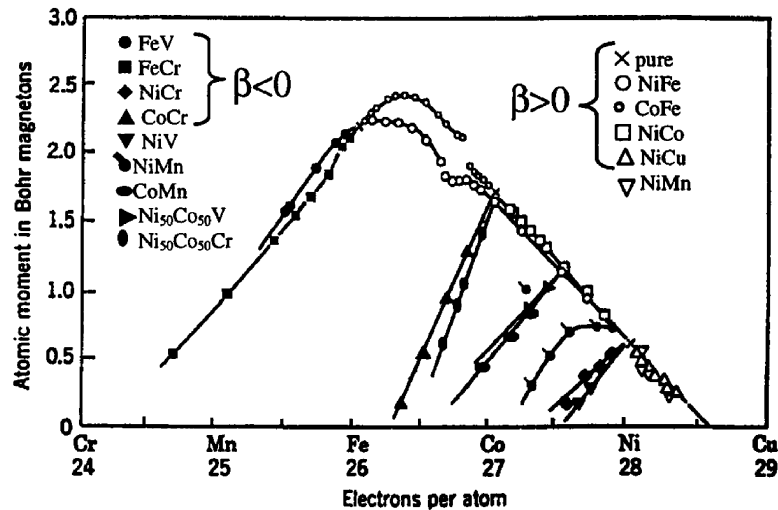


Fig. 6. Slater–Pauling curve for alloys of 3d metals and scattering spin asymmetry. The asymmetry coefficient is positive for pure metals. Fe, Co and Ni and their alloys are located on the slope at -45° and correspond to positive values of β . FeCr, FeV, NiCr and CoCr, are on the branches at $+45^\circ$ and correspond to a negative value of β resulting from the formation of virtual bound states.

multilayers in which impurities (X) are added in the layer F in order to reverse its spin asymmetry [12] and then to reverse the GMR effect. An example is shown in Fig. 5 for NiCr/Cu/Co/Cu multilayers in which Cr impurities have been inserted in order to reverse the asymmetry of the NiCr/Cu layer. At small thicknesses of the NiCr layer, the interface contribution (Ni/Cu) with a positive spin asymmetry is preponderant and the whole asymmetry of the NiCr/Cu layer is of the same sign as the one of the Co/Cu layer, leading to a normal GMR effect. On the contrary, for large thicknesses of the NiCr layer, the bulk contribution dominates, the asymmetry of the NiCr/Cu layer is then negative and opposite to that of the Co/Cu layer, and a reversed GMR effect is obtained. The extensive study performed with different transition metal (F=Fe,Co,Ni) and impurities (X=Fe,Cr,V) has allowed to identify the asymmetry coefficients β of the alloys and the spin asymmetry coefficient γ at the F/Cu interface. The sign of β has been related to the well-known Slater–Pauling curve (Fig. 6). Positive values of β have been obtained when F is a pure metal or an alloy located on the slope at -45° of the Slater–Pauling curve. Negative values of β have been obtained for alloys corresponding to branches with a positive slope (FeCr, FeV, CoCr, CoMn, NiCr). The positive value of β can be related to the small perturbation introduced by the impurity resulting, as in the pure metals, in a density of state (DOS) larger for the minority spin at the Fermi level. In contrast, for Cr, V impurities in Fe, or Cr impurities in Co or Ni, the d levels of the impurity are well above the Fermi level of the matrix and cannot hybridize by the d states of the host. The resonant scattering of the spin \uparrow s electrons

with empty d states of the impurity just above the Fermi level explains the large spin \uparrow resistivity leading to a negative value of β .

3. Magnetization reversal by spin injection

The possibility of reversing the magnetization by a spin-polarized current has been predicted by Slonczewski in 1996 [13]. This phenomenon can be explained by spin accumulation. In fact, if we consider two ferromagnetic layers in the AP state, as shown in Fig. 7, the spin+ direction is the majority one in the first layer and the minority one in the second layer. There is then more spin+ than spin- carrying the current in the first layer and the situation is reversed in the second one. To go to the second layer, spin+ has then to accumulate before reversing in the spin- channel. This spin accumulation extends over a length l_{sf} , called the spin diffusion length. The reversal of the magnetization by spin injection is due to the interaction between the magnetization and the spin accumulation in a direction perpendicular to the magnetization.

In this section, we present results obtained on pillar-shaped Co (15 nm)/Cu (10 nm)/Co (2.5 nm) trilayers [14]. The thick Co layer is the spin injector used to inject spins in the thin layer. The pillars are defined using a complex process including the patterning of the bottom electrode, the fabrication of a template for the pillar by e-beam lithography, the deposition of the trilayer by sputtering into the template, and finally the deposition of the upper Au contact. The pillar has various shapes, from 100×100 to 200×600 nm². Fig. 8 presents an

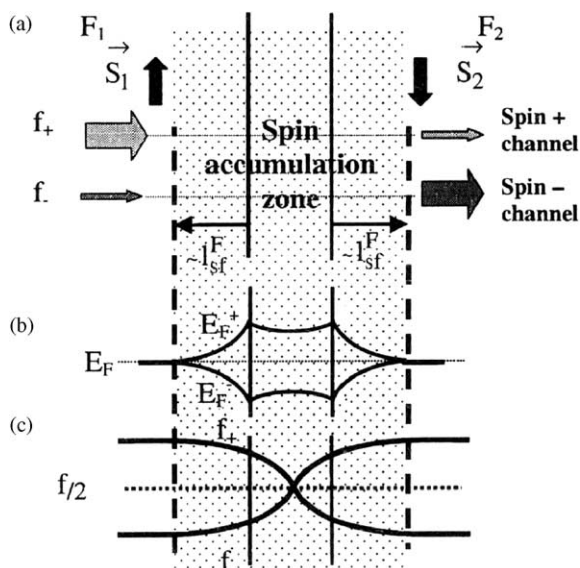


Fig. 7. Illustration of spin accumulation effects in the case of two semi-infinite layers (F_1 and F_2) with opposite spin directions (S_1 and S_2) separated by a thin nonmagnetic layer (NM). Far from NM, in the layer F_1 , the incoming spin+ flux (f_+) is larger than the incoming spin- flux (f_-), whereas the situation is reversed in F_2 ($f_+ < f_-$). The resulting spin accumulation of spin+ electrons extends to about a distance l_{sf} on both sides of NM.

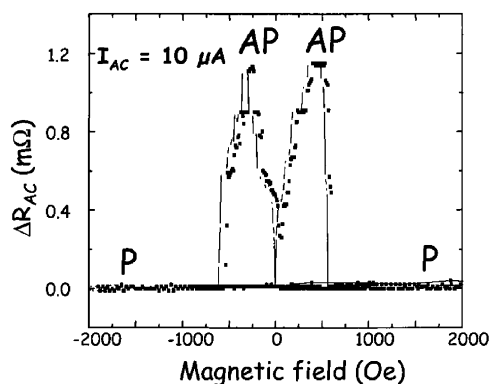


Fig. 8. GMR curve of a $200 \times 600 \text{ nm}^2$ Co/Cu/Co pillar at 4.2 K with $I_{AC} = 50 \mu\text{A}$.

example of CPP-GMR obtained when a small AC current of $50 \mu\text{A}$ is passed through the sample. The GMR is small due to the small contribution of the Co/Cu/Co trilayer to the whole resistance. However, the typical GMR curve obtained for two layers with different coercivities, with well-defined P and AP configurations, is obtained. Fig. 9 represents the variation of the resistance with the intensity of the DC current. Starting at $I = 0$, with the system in the P state,

when a negative current is applied, the system stays in the P state (with the corresponding value R_P of the resistance) until a critical value ($I_{AP} = -I_C$) at which the system switches to the AP state with a resistance R_{AP} . If now, a positive current is applied, the system stays in the AP state (with $R = R_{AP}$) until a value $I_P = I_C$ at which it switches to the P configuration ($R = R_P$). If a magnetic field is applied, I_{AP} increases and I_P decreases, as expected from the stabilization of the P state. The switching from the P to the AP state is induced by a negative current, while the switching from the AP to the P state is induced by a positive current in agreement with the predictions of Slonczewski [13] and the previous results of Katine et al. [15] and rules out the interpretation in terms of magnetic field generated by the applied current.

Another experimental approach appears in Fig. 10. In these experiments, the DC current is fixed and we record GMR curves. In a small DC current (Fig. 10a), the typical GMR curve corresponding to two decoupled magnetic layers is observed. For $I_{DC} = -50 \text{ mA}$, the GMR curve, with a broad peak, is similar to those obtained in multilayers in which a strong antiferromagnetic coupling is present. This clearly confirms that the AP configuration is stabilized by a negative current. For $I_{DC} = 50 \text{ mA}$, the GMR effect disappears as in ferromagnetically coupled multilayers, in agreement with the stabilization of the P state by a positive current. These experimental results can be interpreted in a model [16] combining the Slonczewski's equation of motion [13] with a calculation of the current spin polarization in the Valet-Fert model [17] of the CPP geometry.

4. TMR of magnetic tunnel junctions

TMR is observed in magnetic tunnel junctions combining two ferromagnetic materials separated by a thin insulating barrier. As for the GMR effect, the TMR one results from the variation of the resistance when the magnetic configuration of the magnetizations of the ferromagnetic electrodes goes from AP to P by application of a magnetic field. This property is intensively studied since 1995, when Moodera's group found a large TMR effect at room temperature [18], although the first measurements at low temperature have been performed in 1975. An example of such an effect is shown in Fig. 11, for a Co/ Al_2O_3 /NiFe junction. When the magnetizations of the Co and NiFe layers go from an AP to a P arrangement of the junction decreases. In this example, the effect is 16% at room temperature [19]. Most of the measurements have been performed using an alumina barrier.

In the model of Jullière [20], the TMR ratio is expressed as a function of the spin polarizations SP_1 and

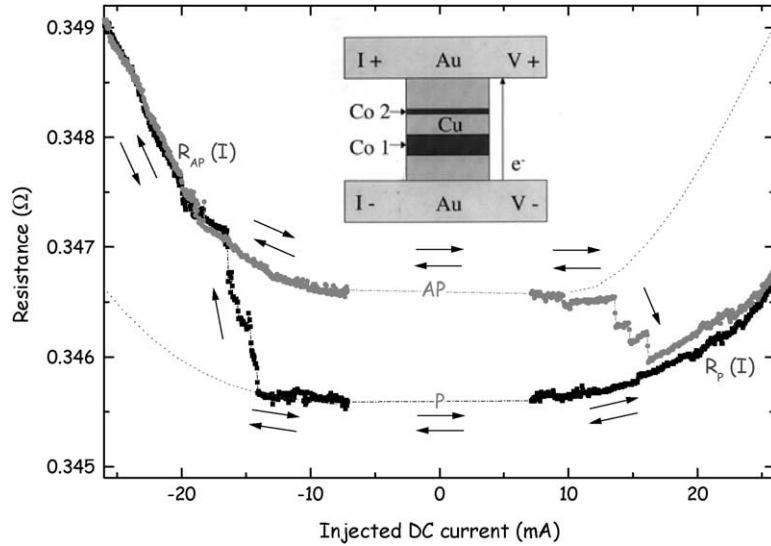


Fig. 9. Resistance as a function of DC current [14].

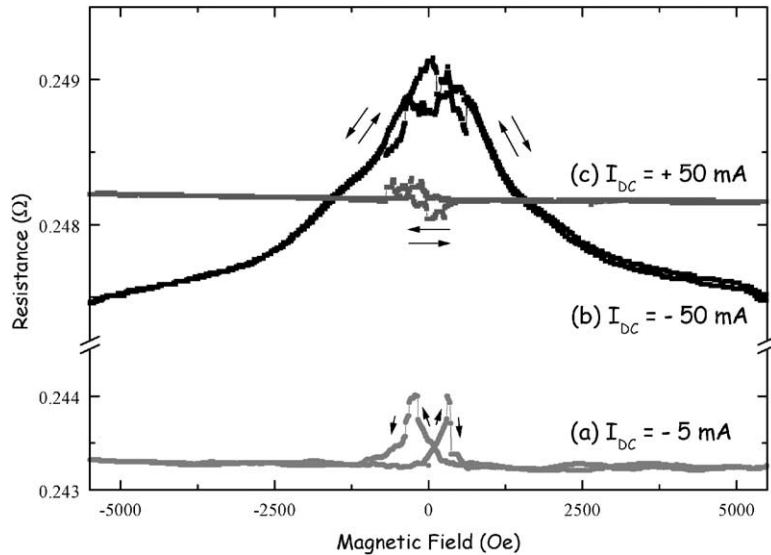


Fig. 10. Resistance as a function of the applied field for a $200 \times 600 \text{ nm}^2$ pillar. The current is -5 mA for curve (a), -50 mA for (b) and $+50 \text{ mA}$ for (c).

SP_2 of the two magnetic electrodes:

$$TMR = \frac{R_{AP} - R_P}{R_{AP}} = \frac{2SP_1SP_2}{1 + SP_1SP_2}$$

with $SP_i = \frac{N_{\uparrow}(E_F) - N_{\downarrow}(E_F)}{N_{\uparrow}(E_F) + N_{\downarrow}(E_F)}$.

This can be explained simply from the scheme in Fig. 12 which represents the case of two half metals (with only one direction at the Fermi level) separated by a thin insulating barrier. In that case, in the AP configuration, transmission from one electrode to the other is not

allowed and the resistance of the junction is infinite. On the contrary, in the P state, transmission occurs and the resistance is finite. This gives for the half-metallic electrodes, a spin polarization equal to 1, a maximum TMR effect of 100%. In the case of transition metal, the effect is more complex to analyze due to the presence of s and d bands at the Fermi level with majority and minority spin directions.

With transition metals, the TMR ratio is limited to 40% at helium temperature and 29% at room temperature. Larger TMR effects have been obtained using half

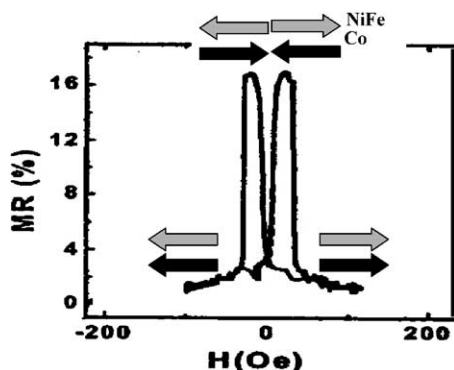


Fig. 11. TMR curve at room temperature of a Co/ALO/NiFe junction [19].

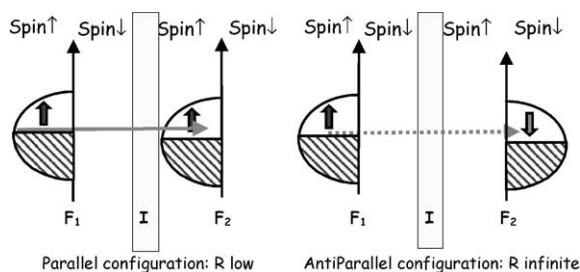


Fig. 12. Schematic picture of the TMR effect in the case of two half-metallic electrodes. The transmission of the electrons from one layer to the other is only possible in the P state resulting in a 100% TMR effect.

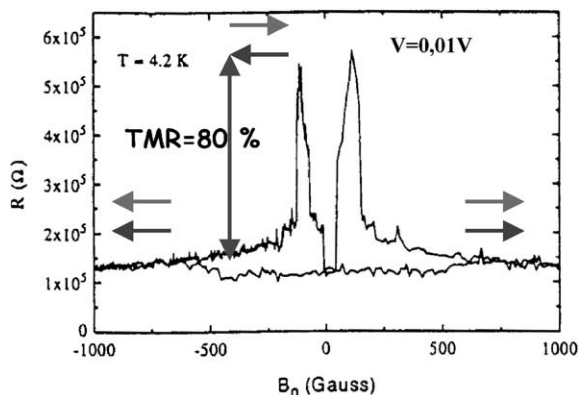


Fig. 13. TMR curve of a LSMO/STO/LSMO junction at 4.2 K. The spin polarization of the LSMO layer is 83%.

metals as electrodes as can be seen in Fig. 13 in the case of a junction with $\text{La}_{0.7}\text{Sr}_{0.3}\text{MnO}_3$ (LSMO) electrodes [21]. The spin polarization deduced from this measurement is 83% if one assumes the same polarization for the two magnetic electrodes. With a polarization of 100% half-metallic compounds allow true on-off operations,

and would be appropriate for gates of nonvolatile logic devices.

Another advantage of half metals is that they can be used as spin analyzers in FM/I/HM tunnel junctions (HM: half metal, I: insulator, FM: ferromagnetic electrode to study) to determine the sign of the spin polarization of the FM element. In fact, if the spin polarization of the HM is known (± 1), the sign of the spin polarization of the FM element can be directly deduced from the shape of the TMR effect. In the case where the spin polarization of the FM electrode is of the same sign as that of the HM, a normal TMR effect, with a resistance smaller in the AP state than in the P state, will be observed and the TMR ratio ($\text{TMR} = 2\text{SP}_{\text{HM}}\text{SP}_{\text{FM}} / (1 + \text{SP}_{\text{HM}}\text{SP}_{\text{FM}})$) will be positive. On the contrary, if the two spin polarizations are of opposite signs, an inverse TMR effect, with a smaller resistance in the AP state, will be observed and the TMR ratio will be negative. LSMO electrode, with a positive spin polarization [22], has been used in that way in Co/I/LSMO tunnel junctions, where I = SrTiO_3 (STO), $\text{Ce}_{1-x}\text{La}_x\text{O}_{2-x}$ (CLO), Al_2O_3 (ALO) or a ALO/STO double barrier [23]. In the case of the ALO barrier (Fig. 14a), a normal TMR effect is observed as leading to a positive value of the spin polarization of the Co as always reported for ALO barriers [24]. But, when the barrier is STO (Fig. 14b) or CLO (Fig. 14c), a reversed TMR effect is obtained. This implies that the spin polarization of the Co is now negative. This clearly evidences that there is no unique polarization for each ferromagnetic metal and the role played by the barrier in magnetic tunnel junctions. The difference between ALO and STO barriers can be accounted for if we consider that the s electrons, with a positive spin polarization, are responsible for the tunneling in the case of an ALO barrier, while the d electrons, with a negative polarization participate predominantly for the tunneling in the case of STO or CLO. Moreover, for the ALO/STO double barrier, the same shape as for the simple ALO barrier is observed (see Fig. 14d), underlying the preponderant role played by the FM/I interface rather than the propagation through the barrier in TMR. These experimental results are in agreement with the recent ab initio calculations of Nguyen Mahn et al. [25] and Oleinik et al. [26,27] who attribute the control of the spin polarization to the bonding at the FM/I interface.

Different barriers produce not only different signs of the spin polarization but also different bias dependence as can be seen in Fig. 15 for ALO/STO and STO barriers in Co/I/LSMO junctions. For the ALO/STO barrier (Fig. 15a), a classical rapid decrease of the TMR is observed as always observed for ALO barrier. On the contrary, for the junction with an STO barrier (Fig. 15b), an asymmetric bias dependence between positive and negative applied voltage is observed. The TMR bias dependence at negative bias (that is electron

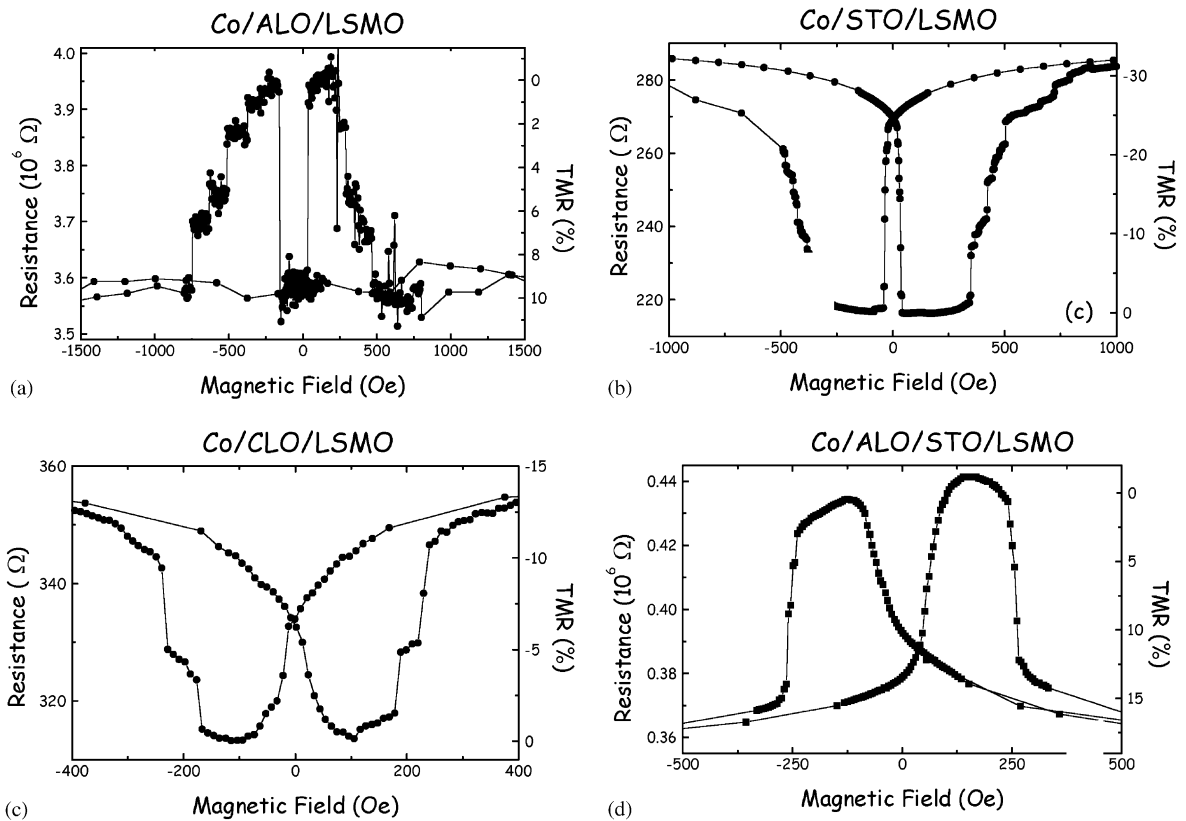


Fig. 14. TMR curves of four Co/I/LSMO tunnel junctions at 40K with I = (a) ALO, (b) STO, (c) CLO and (d) ALO/STO [23].

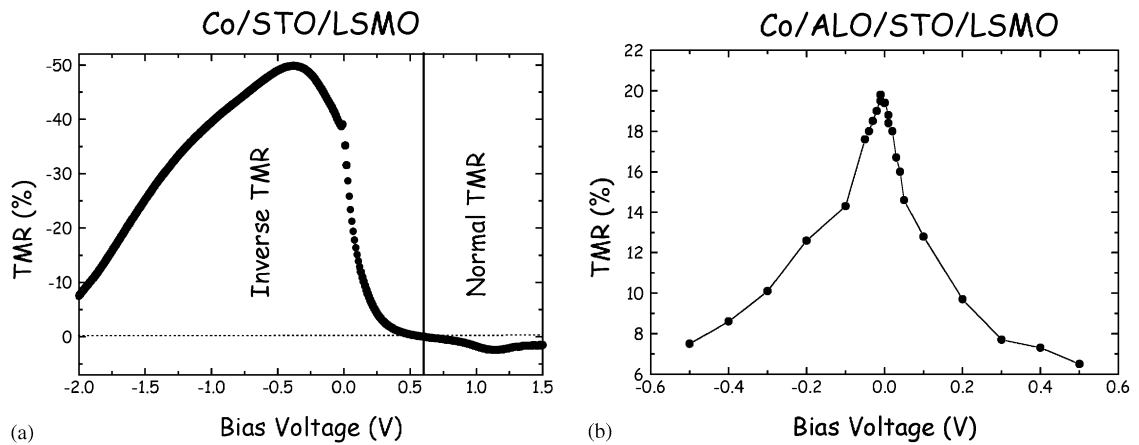


Fig. 15. Bias dependence of the TMR at 40K for Co/STO/LSMO and Co/ALO/STO/LSMO tunnel junctions.

flowing from LSMO to Co) reflects quite well the DOS of the Co d band, with an increase of the reverse TMR effect between zero bias and -0.4 V corresponding to an increase of the DOS of the Co d_{\downarrow} band, a maximum

at -0.4 V corresponding to a maximum in the DOS of the Co d_{\downarrow} band and a decrease at more negative bias corresponding to the decrease in the d_{\downarrow} DOS of the Co. It is to be noted that the absence of substructure in the

case of the ALO barrier could also be produced by the amorphous character of the barrier.

5. Conclusion

We have described three different topics in the field of spin electronics, that is the GMR of magnetic multilayers, the TMR of magnetic tunnel junctions and the possibility to reverse the magnetization by spin injection. Two of these effects, GMR and more recently TMR, have already yielded applications in the field of magnetic sensors and read heads for magnetic hard disk drives. Nonvolatile magnetic memory (MRAM) will appear in the market in the near future. The integration of half metals in these structures will give rise to a new application of spin electronics as nonvolatile reprogrammable logic compounds.

References

- [1] M. Baibich, J.M. Broto, A. Fert, F.N. Guyen Van Dau, F. Petroff, P. Etienne, G. Creuzet, A. Friederich, Phys. Rev. Lett. 61 (1988) 2472.
- [2] P. Grünberg, R. Schreiber, Y. Pang, M.B. Brodsky, H. Sowers, Phys. Rev. Lett. 57 (1986) 2442.
- [3] R. Schad, C.D. Potter, P. Beliën, G. Verbanck, V.V. Moshchalkov, Y. Bruynseraede, Appl. Phys. Lett. 64 (1994) 3500.
- [4] A. Barthélémy, A. Fert, F. Petroff, Handbook of Magnetic Materials, Vol. 12, Elsevier, Amsterdam, 1999, pp. 1–96.
- [5] D.H. Mosca, F. Petroff, A. Fert, P.A. Schroeder, W.P. Pratt, R. Loloee, J. Magn. Magn. Mater. 94 (1991) L1.
- [6] J. Barnas, A. Fuss, R.E. Camley, P. Grünberg, W. Zinn, Phys. Rev. B 42 (1990) 8110.
- [7] B. Dieny, V.S. Speriosu, S.S.P. Parkin, B.A. Gurney, D.R. Wilhoit, D. Mauri, Phys. Rev. B 43 (1991) 1297.
- [8] W.P. Pratt, S.F. Lee, J.M. Slaughter, R. Loloee, P.A. Schroeder, J. Bass, Phys. Rev. Lett. 66 (1991) 3060.
- [9] P.A. Schroeder, J. Bass, P. Holody, S.F. Lee, R. Loloee, W.P. Pratt Jr., Q. Yang, Magnetic Ultrathin Films, Multilayers and Surfaces. Interfaces and Characterization. Materials Research Society Symposium Proceedings, Vol. 313, MRS, Pittsburg, PA, 1993, p. 47.
- [10] A. Fert, L. Piraux, J. Magn. Magn. Mat. 200 (1999) 338 (Special issue).
- [11] M.A.M. Gijs, M.T. Johnson, A. Reinders, P.E. Huisman, R.J.M. van de Veerdonk, S.K.J. Lenczowski, R.M.J. Gansewinkel, Appl. Phys. Lett. 66 (1995) 1839.
- [12] C. Vouille, A. Barthélémy, A. Fert, P.A. Schroeder, S.H. Hsu, A. Reilly, R. Loloee, Phys. Rev. B 60 (1999) 6710.
- [13] J. Slonczewski, J. Magn. Magn. Mater. 159 (1996) 1.
- [14] J. Grollier, V. Cros, A. Hamzic, J.M. George, H. Jaffrès, A. Fert, G. Faini, J. Ben Youssef, H. Legall, Appl. Phys. Lett. 78 (2001) 3663.
- [15] A. Katine et al, Phys. Rev. Lett. 84 (2000) 3149; F.J. Albert, J.A. Katine, R.A. Burhman, D.C. Ralph, Appl. Phys. Lett. 77 (2000) 3809.
- [16] A. Fert, A. Barthélémy, J. Ben Youssef, J-P. Contour, V. Cros, J.M. De Teresa, A. Hamzic, J.M. George, G. Faini, J. Grollier, H. Jaffrès, H. Le Gall, F. Montaigne, F. Pailloux, F. Petroff, Mater. Sci. Eng. B 84 (2001) 1–9.
- [17] T. Valet, A. Fert, Phys. Rev. B 48 (1993) 7099.
- [18] J. Moodera, L.R. Kinder, R.M. Wong, R. Meservey, Phys. Rev. Lett. 74 (1995) 3273.
- [19] J. Nassar, M. Hehn, A. Vaures, F. Petroff, A. Fert, Appl. Phys. Lett. 73 (1998) 698.
- [20] R. Jullière, Phys. Lett. A 54 (1975) 225.
- [21] J. Nassar, M. Viret, M. Drouet, J.P. Contour, C. Fermon, A. Fert, Mat. Res. Soc. Symp. Proc. 494 (1998) 231.
- [22] D.C. Worledge, T.H. Geballe, Appl. Phys. Lett. 76 (2000) 900.
- [23] J.M. De Teresa, A. Barthélémy, A. Fert, J.P. Contour, F. Montaigne, P. Seneor, Science 286 (1999) 507.
- [24] R. Meservey, P.M. Tedrow, Phys. Rep. 238 (1994) 173.
- [25] D. Nguyen-Mahn, E.Y. Tsymbal, D.G. Pettifor, C. Arcangeli, R. Tank, O.K. Andersen, A. Pasturel, Mat. Res. Soc. Symp. Proc. 492 (1998) 319.
- [26] I.I. Oleinik, E.Y. Tsymbal, D.G. Pettifor, Phys. Rev. B 62 (2000) 3952.
- [27] I.I. Oleinik, E.Y. Tsymbal, D.G. Pettifor, Phys. Rev. B 65 (2001) 020401R.